
Abstract

Sammendrag

Preface

Table of Contents

List of Figures	ix
List of Tables	xi
Notation	xiii
1 Introduction	1
2 Theory	3
2.1 The type of flow systems considered	3
2.2 Definition of Lagrangian coherent structures for three-dimensional flows	4
2.2.1 Hyperbolic LCSs	5
3 Method	7
3.1 Arnold-Beltrami-Childress flow	7
3.1.1 (Normal) vector field for a sinusoidal surface	8
3.2 The method of geodesic level sets	8
4 Results	11
5 Discussion	19
6 Conclusions	21
References	23
A Appendix A	25

List of Figures

2.1	Geometric interpretation of the eigenvectors of the Cauchy-Green strain tensor	4
3.1	Geometric interpretation of the eigenvectors of the Cauchy-Green strain tensor	8
3.2	Geometric interpretation of the eigenvectors of the Cauchy-Green strain tensor	9
4.1	Veni, vidi, Aviici	11
4.2	Veni, vidi, Aviici	12
4.3	Veni, vidi, Aviici	12
4.4	Veni, vidi, Aviici	13
4.5	Veni, vidi, Aviici	13
4.6	Aviici is love, Aviici is life	13
4.7	Aviici is love, Aviici is life	14
4.8	Veni, vidi, Aviici	14
4.9	Aviici is love, Aviici is life	15
4.10	Aviici is love, Aviici is life	15
4.11	Aviici is love, Aviici is life	16
4.12	Aviici is love, Aviici is life	16
4.13	Aviici is love, Aviici is life	17
4.14	Aviici is love, Aviici is life	17
4.15	Aviici is love, Aviici is life	18

List of Tables

Notation

Newton's notation is used for differentiation with respect to time, i.e.:

$$\dot{f}(t) \equiv \frac{df(t)}{dt}.$$

Vectors are denoted by lowercase, upright, bold letters, like this:

$$\xi = (\xi_1, \xi_2, \dots, \xi_n).$$

The Euclidean norm of a vector $\xi \in \mathbb{R}^n$ is denoted by:

$$\|\xi\| = \sqrt{\xi_1^2 + \xi_2^2 + \dots + \xi_n^2}.$$

Matrices and matrix representations of rank-2 tensors are denoted by uppercase, upright, bold letters, as follows:

$$\mathbf{A} = (a_{i,j}) = \begin{pmatrix} a_{1,1} & a_{1,2} & \dots & a_{1,n} \\ a_{2,1} & a_{2,2} & \dots & a_{2,n} \\ \vdots & \vdots & \ddots & \vdots \\ a_{m,1} & a_{m,2} & \dots & a_{m,n} \end{pmatrix}.$$

1 Introduction

2 Theory

2.1 THE TYPE OF FLOW SYSTEMS CONSIDERED

We consider flow in three-dimensional dynamical systems of the form

$$\dot{\mathbf{x}} = \mathbf{v}(t, \mathbf{x}), \quad \mathbf{x} \in \mathcal{U}, \quad t \in [t_0, t_1], \quad (2.1)$$

i.e., systems defined for the finite time interval $[t_0, t_1]$ on an open, bounded subset \mathcal{U} of \mathbb{R}^3 . In addition, the velocity field \mathbf{v} is assumed to be smooth in its arguments. Depending on the exact nature of the velocity field \mathbf{v} , analytical particle trajectories, that is, analytical solutions of system (2.1), may or may not exist. The flow particles are assumed to be infinitesimal and massless, i.e., non-interacting *tracers* of the overall circulation.

Letting $\mathbf{x}(t; t_0, \mathbf{x}_0)$ denote the trajectory of a tracer in the system given by equation (2.1), the flow map is defined as

$$\Phi_{t_0}^t(\mathbf{x}_0) = \mathbf{x}(t; t_0, \mathbf{x}_0), \quad (2.2)$$

hence, the flow map describes the movement of tracers from one point in time to another mathematically. In general, the flow map is as smooth as the underlying velocity field (cf. system (2.1)) (Farazmand and Haller 2012a). For sufficiently smooth velocity fields, the right Cauchy-Green strain tensor field can be defined as

$$\mathbf{C}_{t_0}^t(\mathbf{x}_0) = \left(\nabla \Phi_{t_0}^t(\mathbf{x}_0) \right)^* \left(\nabla \Phi_{t_0}^t(\mathbf{x}_0) \right), \quad (2.3)$$

where $\nabla \Phi_{t_0}^t$ denotes the Jacobian matrix of the flow map $\Phi_{t_0}^t$, and the asterisk refers to the adjoint operation, which, because the Jacobian $\nabla \Phi_{t_0}^t$ is real-valued, equates to matrix transposition. Component-wise, the Jacobian matrix of a general vector-valued function \mathbf{f} is defined as

$$(\nabla \mathbf{f})_{i,j} = \frac{\partial f_i}{\partial x_j}, \quad \mathbf{f} = \mathbf{f}(\mathbf{x}) = (f_1(\mathbf{x}), f_2(\mathbf{x}), \dots), \quad (2.4)$$

which, for our three-dimensional flow, reduces to

$$\nabla \mathbf{f} = \begin{pmatrix} \frac{\partial f_1}{\partial x} & \frac{\partial f_1}{\partial y} & \frac{\partial f_1}{\partial z} \\ \frac{\partial f_2}{\partial x} & \frac{\partial f_2}{\partial y} & \frac{\partial f_2}{\partial z} \\ \frac{\partial f_3}{\partial x} & \frac{\partial f_3}{\partial y} & \frac{\partial f_3}{\partial z} \end{pmatrix}. \quad (2.5)$$

Because the Jacobian of the flow map is invertible, the Cauchy-Green strain tensor $\mathbf{C}_{t_0}^t$ is symmetric and positive definite (Farazmand and Haller 2012a). Thus, it has three real, positive eigenvalues and orthogonal, real eigenvectors. Its eigenvalues λ_i and corresponding unit eigenvectors ξ_i are defined by

$$\mathbf{C}_{t_0}^t(\mathbf{x}_0) \xi_i(\mathbf{x}_0) = \lambda_i \xi_i(\mathbf{x}_0), \quad \|\xi_i(\mathbf{x}_0)\| = 1, \quad i = 1, 2, 3, \quad (2.6)$$

$$0 < \lambda_1(\mathbf{x}_0) \leq \lambda_2(\mathbf{x}_0) \leq \lambda_3(\mathbf{x}_0),$$

where, for the sake of notational transparency, the dependence of λ_i and ξ_i on t_0 and t has been suppressed. The geometric interpretation of equation (2.6) is that a fluid element undergoes the most stretching along the ξ_3 axis, less stretching along the ξ_2 axis, and the least stretching along the ξ_1 axis. This concept is shown in figure 2.1.

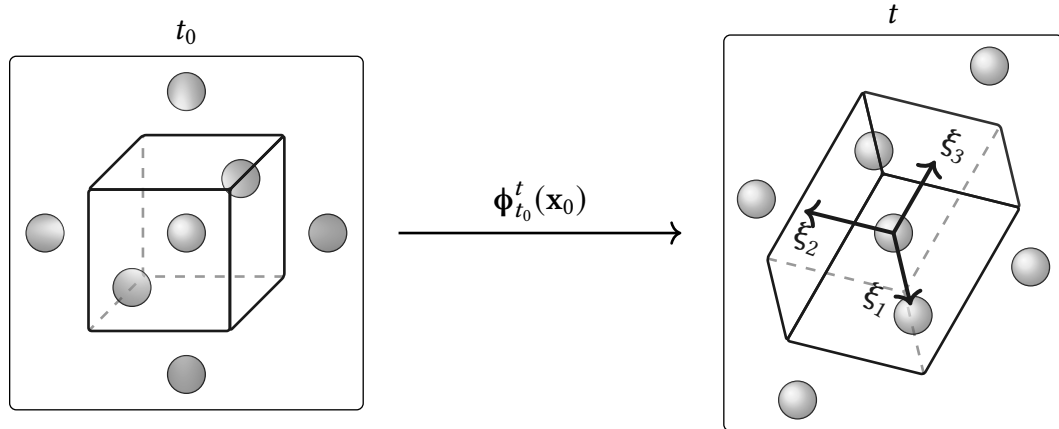


Figure 2.1: Geometric interpretation of the eigenvectors of the Cauchy-Green strain tensor. The central unit cell is stretched and deformed under the flow map $\phi_{t_0}^t(\mathbf{x}_0)$. The local stretching is the largest in the direction of ξ_3 , the eigenvector which corresponds to the largest eigenvalue, λ_3 , of the Cauchy-Green strain tensor, defined in equation (2.6). Along the ξ_i axes, the stretch factors are given by $\sqrt{\lambda_i}$, respectively.

As the stretch factors along the ξ_i axes are given by the square roots of the corresponding eigenvalues, for incompressible flow, the eigenvalues satisfy

$$\lambda_1(\mathbf{x}_0)\lambda_2(\mathbf{x}_0)\lambda_3(\mathbf{x}_0) = 1 \quad \forall \mathbf{x}_0 \in \mathcal{U}, \quad (2.7)$$

where, in the context of tracer advection, incompressibility is equivalent to the velocity field \mathbf{v} being divergence-free (i.e., $\nabla \cdot \mathbf{v} \equiv 0$ in system (2.1)).

2.2 DEFINITION OF LAGRANGIAN COHERENT STRUCTURES FOR THREE-DIMENSIONAL FLOWS

Lagrangian coherent structures (henceforth abbreviated to LCSs) can be described as time-evolving surfaces which shape coherent trajectory patterns in dynamical systems, defined over a finite time interval (Haller 2010). There are three main types of LCSs, namely *elliptic*, *hyperbolic* and *parabolic*. Roughly speaking, parabolic LCSs outline cores of jet-like trajectories, elliptic LCSs describe vortex boundaries, whereas hyperbolic LCSs are comprised of overall attractive or repelling manifolds. As such, hyperbolic LCSs practically act as organizing centers of observable tracer patterns (Onu, Huhn, and Haller 2015). Because hyperbolic LCSs provide the most readily applicable insight in terms of forecasting flow in e.g. oceanic currents, such structures have been the focus of this project.

2.2.1 Hyperbolic LCSs

The identification of LCSs for reliable forecasting requires sufficiency and necessity conditions, supported by mathematical theorems. Haller (2010) derived a variational LCS theory based on the Cauchy-Green strain tensor, defined by equation (2.3), from which the aforementioned conditions follow. The immediately relevant parts of Haller's theory are given in definitions 1–4 (Haller 2010).

Definition 1 (*Normally repellent material surfaces*).

A *normally repellent material surface* over the time interval $[t_0, t_0 + T]$ is a compact material surface segment $\mathcal{M}(t)$ which is overall repelling, and on which the normal repulsion rate is greater than the tangential repulsion rate.

A *material surface* is a smooth surface $\mathcal{M}(t_0)$ at time t_0 , which is advected by the flow map, given by equation (2.2), into a dynamic material line $\mathcal{M}(t) = \Phi_{t_0}^t(\mathcal{M}(t_0))$. The required *compactness* of the material surface segment signifies that, in some sense, it must be topologically well-behaved. That the material surface is *overall repelling* means that nearby trajectories are repelled from, rather than attracted towards, the material surface. Lastly, requiring that the *normal* repulsion rate is greater than the *tangential* repulsion rate means that nearby trajectories are in fact driven away from the material surface, rather than being stretched along with it due to shear stress.

Definition 2 (*Repelling LCS*).

A *repelling LCS* over the time interval $[t_0, t_0 + T]$ is a normally repelling material surface $\mathcal{M}(t_0)$ whose normal repulsion admits a pointwise non-degenerate maximum relative to any nearby material surface $\widehat{\mathcal{M}}(t_0)$.

Definition 3 (*Attracting LCS*).

An *attracting LCS* over the time interval $[t_0, t_0 + T]$ is defined as a repelling LCS over the *backward* time interval $[t_0 + T, t_0]$.

Definition 4 (*Hyperbolic LCS*).

A *hyperbolic LCS* over the time interval $[t_0, t_0 + T]$ is a *repelling* or *attracting* LCS over the same time interval.

Note that the above definitions associate LCSs with the time interval I over which the dynamical system under consideration is known, or, at the very least, where information regarding the behaviour of tracers, is sought. Generally, LCSs obtained over a time interval I do not necessarily exist over different time intervals (Farazmand and Haller 2012a).

For sufficiently smooth three-dimensional flow, the above definitions can be summarized as a set of mathematical existence criteria, based on the Cauchy-Green strain tensor (Haller 2010; Farazmand and Haller 2012a; Karrasch 2012; Farazmand and Haller 2012b). These are given in theorem 1.

Theorem 1 (Sufficient and necessary conditions for LCSs in three-dimensional flows). Consider a compact material surface $\mathcal{M}(t) \subset \mathcal{U}$ evolving over the time interval $[t_0, t_0 + T]$. Then $\mathcal{M}(t)$ is a repelling LCS over $[t_0, t_0 + T]$ if and only if all of the following holds for all initial conditions $\mathbf{x}_0 \in \mathcal{M}(t_0)$:

$$\lambda_2(\mathbf{x}_0) \neq \lambda_3(\mathbf{x}_0) > 1, \quad (2.8a)$$

$$\left\langle \xi_3(\mathbf{x}_0), \mathbf{H}_{\lambda_3}(\mathbf{x}_0) \xi_3(\mathbf{x}_0) \right\rangle < 0 \quad (2.8b)$$

$$\xi_3(\mathbf{x}_0) \perp \mathcal{M}(t_0), \quad (2.8c)$$

$$\left\langle \nabla \lambda_3(\mathbf{x}_0), \xi_3(\mathbf{x}_0) \right\rangle = 0. \quad (2.8d)$$

In theorem 1, $\langle \cdot, \cdot \rangle$ signifies the Euclidean inner product, and \mathbf{H}_{λ_3} denotes the Hessian matrix of the largest eigenvalues of the Cauchy-Green strain tensor field. Component-wise, the Hessian matrix of a general, smooth, scalar-valued function f is defined as

$$(\mathbf{H}_f)_{i,j} = \frac{\partial^2 f}{\partial x_i \partial x_j}, \quad (2.9)$$

which, for our three-dimensional flow, reduces to

$$\mathbf{H}_f = \begin{pmatrix} \frac{\partial^2 f}{\partial x^2} & \frac{\partial^2 f}{\partial x \partial y} & \frac{\partial^2 f}{\partial x \partial z} \\ \frac{\partial^2 f}{\partial y \partial x} & \frac{\partial^2 f}{\partial y^2} & \frac{\partial^2 f}{\partial y \partial z} \\ \frac{\partial^2 f}{\partial z \partial x} & \frac{\partial^2 f}{\partial z \partial y} & \frac{\partial^2 f}{\partial z^2} \end{pmatrix}. \quad (2.10)$$

Condition (2.8a) ensures that the normal repulsion rate is larger than the tangential stretch due to shear strain along the LCS, in accordance with definition 1. Conditions (2.8c) and (2.8d) suffice to enforce that the normal repulsion rate attains a local extremum along the LCS, relative to all nearby material surfaces. Lastly, condition (2.8b) ensures that this is a strict local maximum.

Forslag til teori-outlines

- Interpolasjon
- Integrasjon
- Cauchy-Green
- Variasjonsligning
- LCS, spesifikt hyperbolske i 3D
- Hva er en mangfoldighet?
- Oettingers argument del 2

3 Method

In order to identify LCSs in three-dimensional flow by means of geodesic level set approximations, a system which has been studied extensively in the literature was chosen. The system is a simple example of a fluid flow which can exhibit chaotic behaviour (Frisch 1995, p.204).

3.1 ARNOLD-BELTRAMI-CHILDRESS FLOW

The Arnold-Beltrami-Childress (hereafter abbreviated to ABC) flow is a three-dimensional incompressible velocity field which solves the Euler equations exactly. In terms of the Cartesian coordinate vector $\mathbf{x} = (x, y, z)$, the system can be expressed mathematically as

$$\dot{\mathbf{x}} = \mathbf{v}(t, \mathbf{x}) = \begin{pmatrix} A \sin(z) + C \cos(y) \\ B \sin(x) + A \cos(z) \\ C \sin(y) + B \cos(x) \end{pmatrix}, \quad (3.1)$$

where A , B and C are spatially invariant parameters which dictate the nature of the flow pattern. The inherent periodicity with regards to the Cartesian coordinates naturally leads to a domain of interest $\mathcal{U} = [0, 2\pi]^3$ with periodic boundary conditions imposed along all three Cartesian axes.

For stationary flow, the parameter values

$$A = \sqrt{3}, \quad B = \sqrt{2}, \quad C = 1 \quad (3.2)$$

were used, as has been common in the literature, for instance in the article by Oettinger and Haller (2016), as these values are known for exhibiting chaotic trajectories (Zhao et al. 1993).

Rundt her kan sikkert språket forbedres / brødtekst genereres. Lar det være et problem for fremtidige A.

In order to enforce chaotic behaviour, the parameters A , B and C can be modified to be temporally aperiodic as follows:

$$\begin{aligned} A &= \sqrt{3}, \\ B &= \sqrt{2} [1 + k_0 \tanh(k_1 t) \cos((k_2 t)^2)], \\ C &= 1 + k_0 \tanh(k_1 t) \sin((k_3 t)^2), \end{aligned} \quad (3.3)$$

where the parameter values

$$k_0 = 0.3, \quad k_1 = 0.5, \quad k_2 = 1.5, \quad k_3 = 1.8 \quad (3.4)$$

were used, like in Oettinger and Haller (2016).

3.1.1 (Normal) vector field for a sinusoidal surface

For the surface implicitly defined as the zeros of the function

$$f(\mathbf{r}) = A \sin(\omega_x x) \sin(\omega_y y) + (z_0 - z), \quad (3.5)$$

one possible choice for its normal vector field is

$$\mathbf{n}(\mathbf{r}) = \begin{pmatrix} A\omega_x \cos(\omega_x x) \sin(\omega_y y) \\ A\omega_y \sin(\omega_x x) \cos(\omega_y y) \\ -1 \end{pmatrix}. \quad (3.6)$$

3.2 THE METHOD OF GEODESIC LEVEL SETS

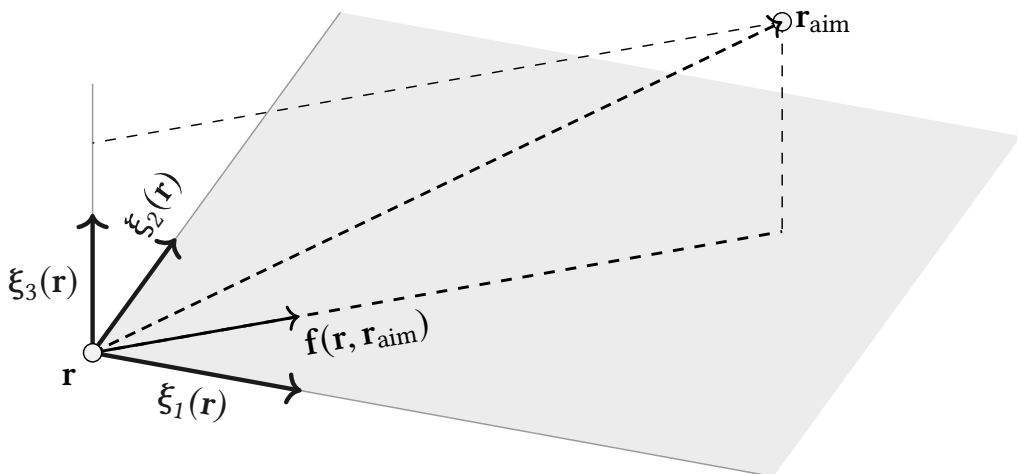


Figure 3.1: Geometric interpretation of the eigenvectors of the Cauchy-Green strain tensor. The central unit cell is stretched and deformed under the flow map $\phi_{t_0}^t(\mathbf{x}_0)$. The local stretching is the largest in the direction of ξ_3 , the eigenvector which corresponds to the largest eigenvalue, λ_3 , of the Cauchy-Green strain tensor, defined in equation (2.6). Along the ξ_i axes, the stretch factors are given by $\sqrt{\lambda_i}$, respectively.

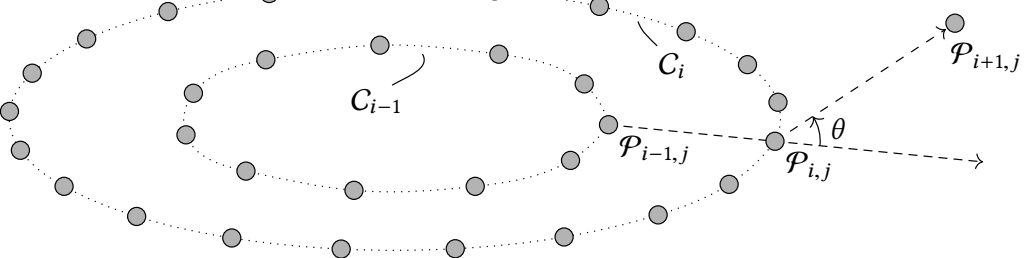


Figure 3.2: Geometrix interpretation of the eigenvectors of the Cauchy-Green strain tensor. The central unit cell is stretched and deformed under the flow map $\Phi_{t_0}^t(\mathbf{x}_0)$. The local stretching is the largest in the direction of ξ_3 , the eigenvector which corresponds to the largest eigenvalue, λ_3 , of the Cauchy-Green strain tensor, defined in equation (2.6). Along the ξ_i axes, the stretch factors are given by $\sqrt{\lambda_i}$, respectively.

4 Results

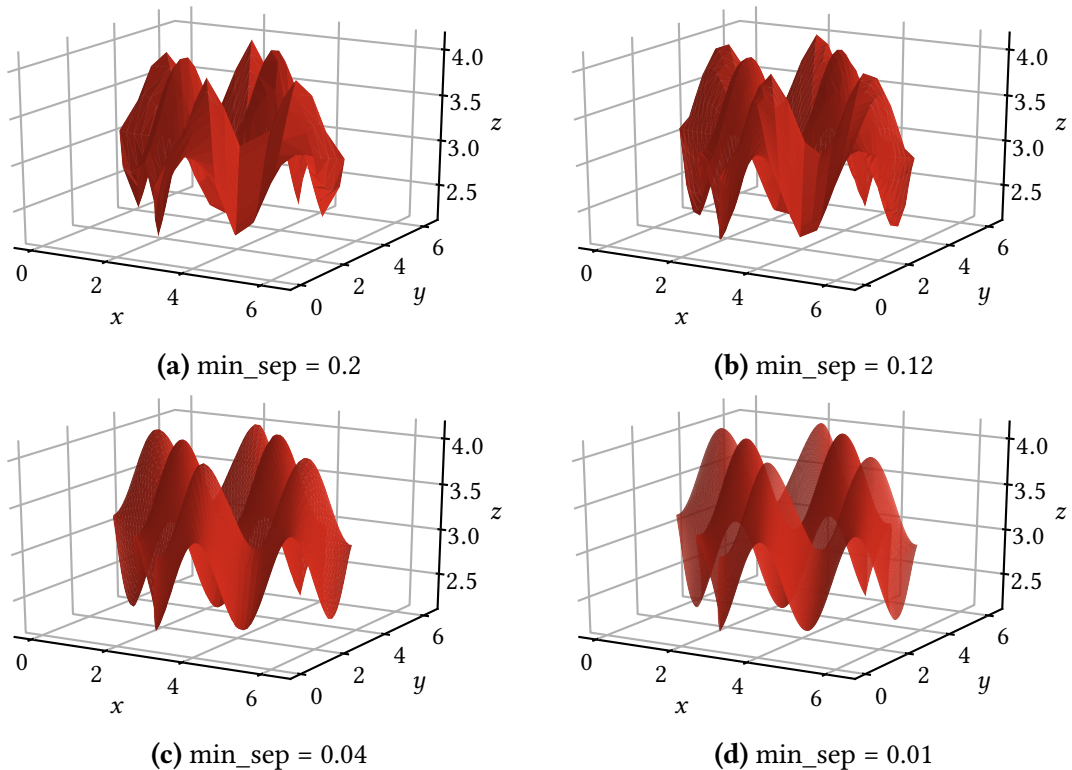


Figure 4.1: Manifolds generated from analytically determined vector field.

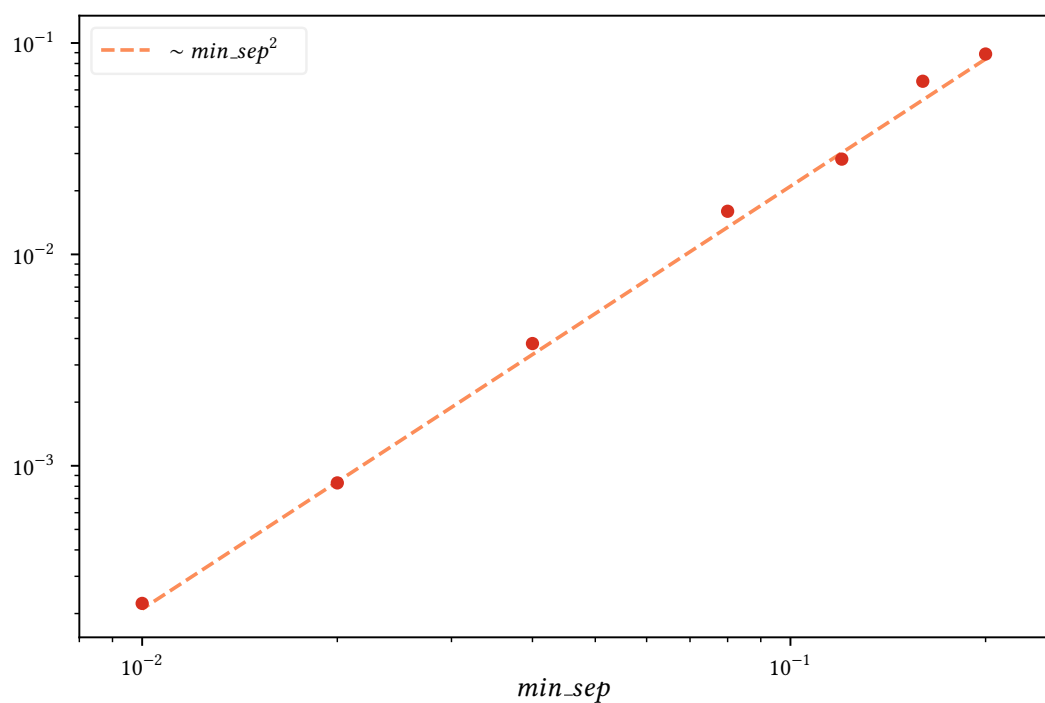


Figure 4.2: RMS error of sinusoidal manifolds

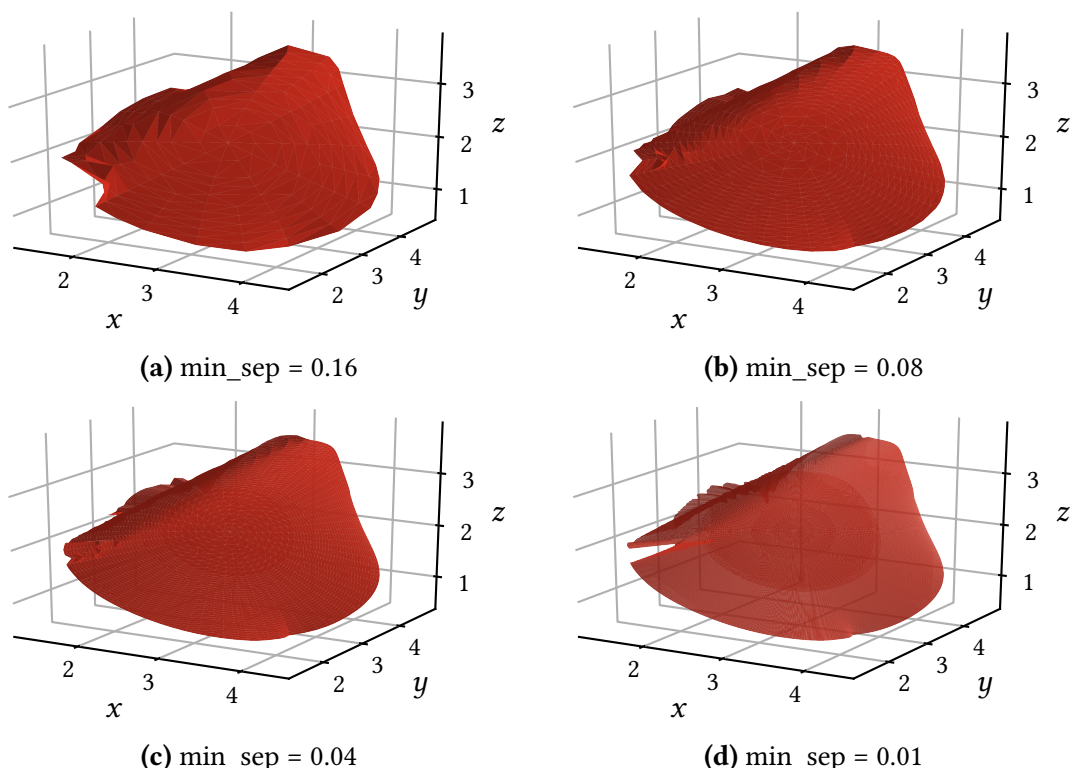
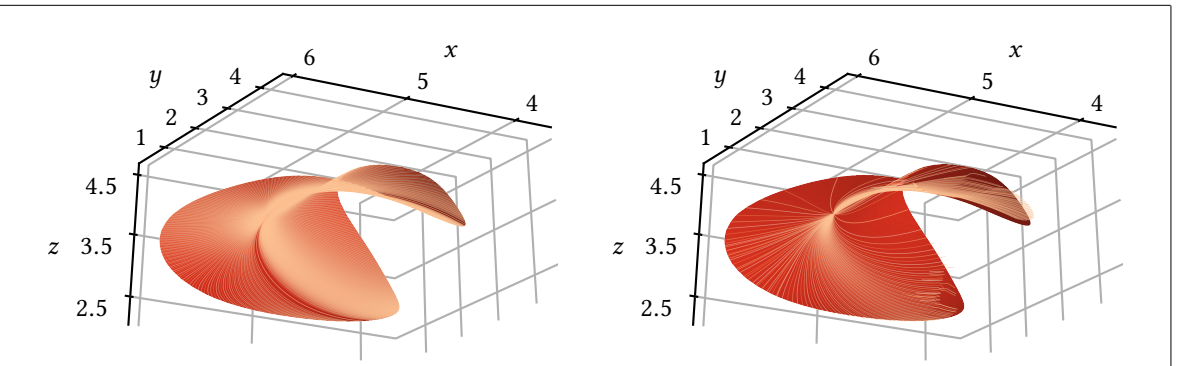
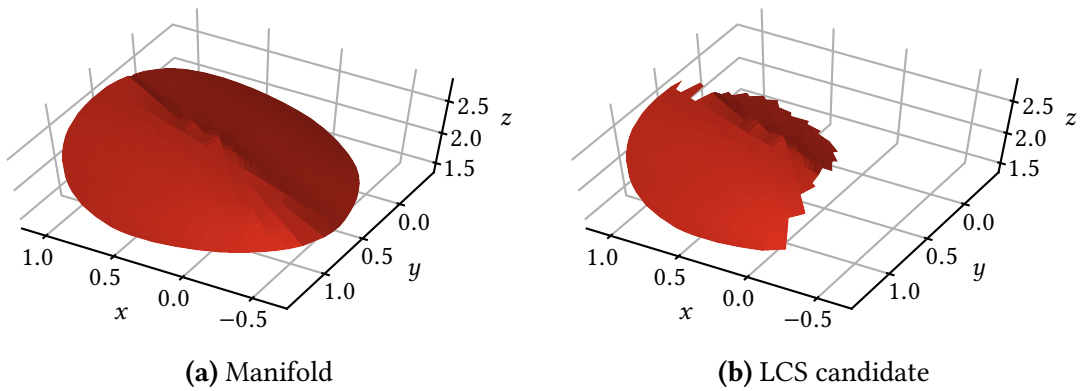


Figure 4.3: Numerical convergence as min_sep decreases



(a) Trajectories forced radially outwards (b) Pure linear combinations of ξ_1 and ξ_2

Figure 4.4: Trajectories with local directionality given by linear combinations of ξ_1 and ξ_2 .



(a) Manifold (b) LCS candidate

Figure 4.5: Converting a manifold to an LCS candidate

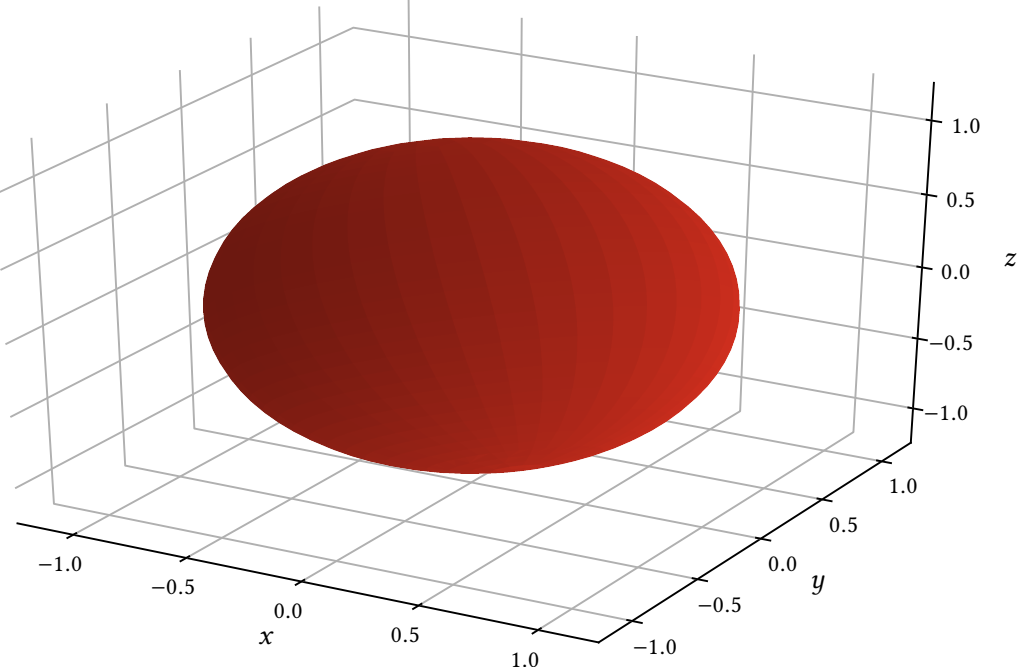


Figure 4.6: The identified LCS for the spherical flow

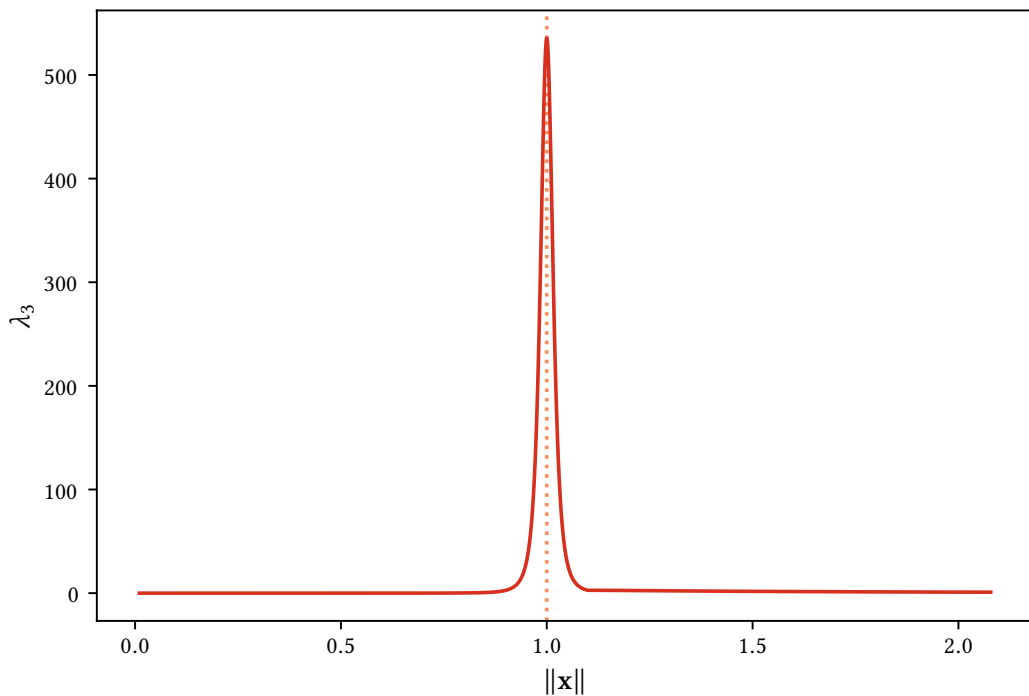


Figure 4.7: λ_3 as a function of radius, for the spherical flow. Displayed here is the arithmetic average across all solid angles.

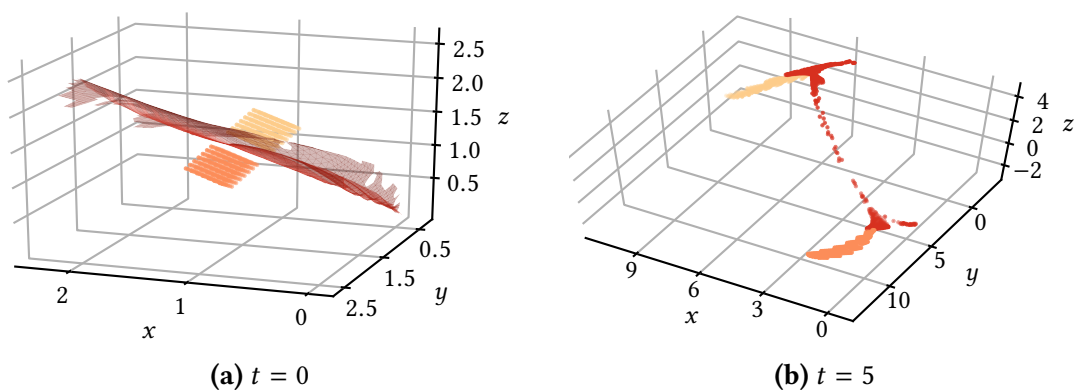


Figure 4.8: Blob test for verifying expected LCS behaviour

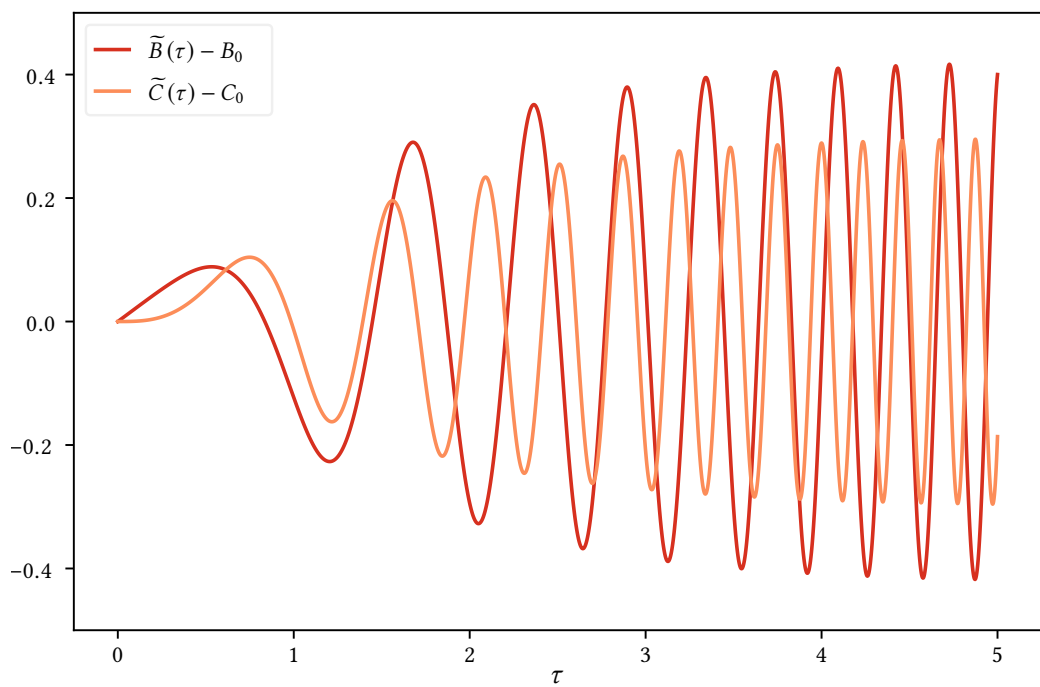


Figure 4.9: Time evolution of nonstationary ABC coefficients

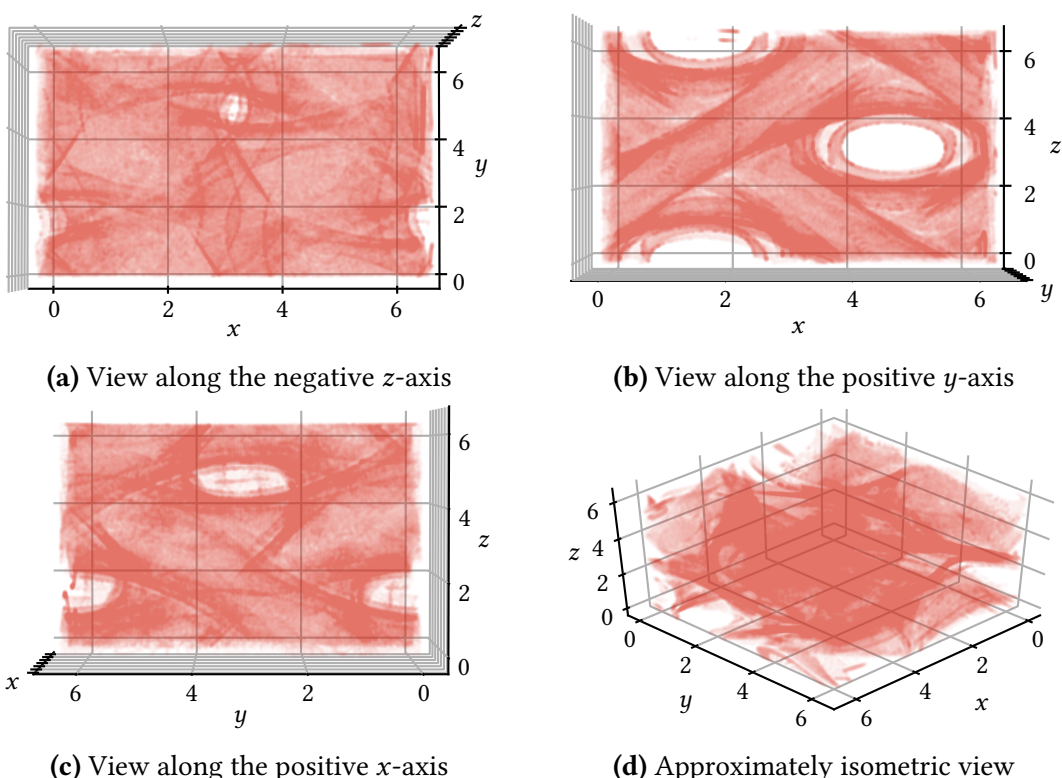


Figure 4.10: ABD domain obtained for stationary flow. $\epsilon = 0.005$.

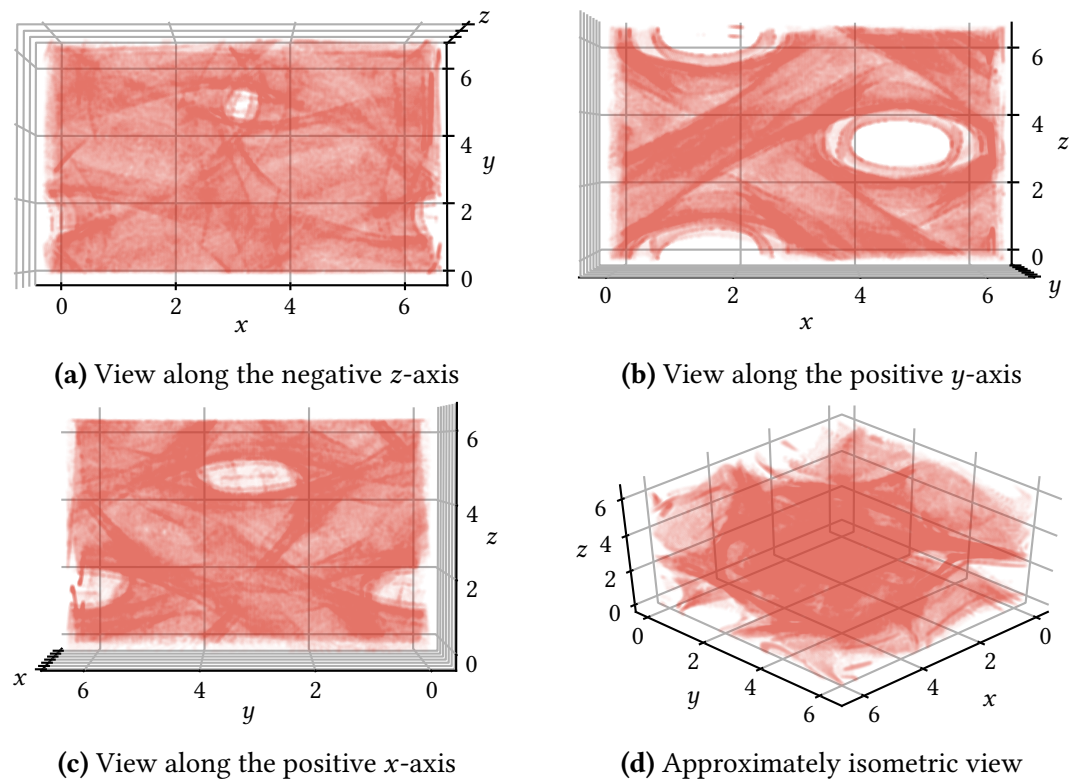


Figure 4.11: ABD domain obtained for dynamic flow. $\epsilon = 0.005$.

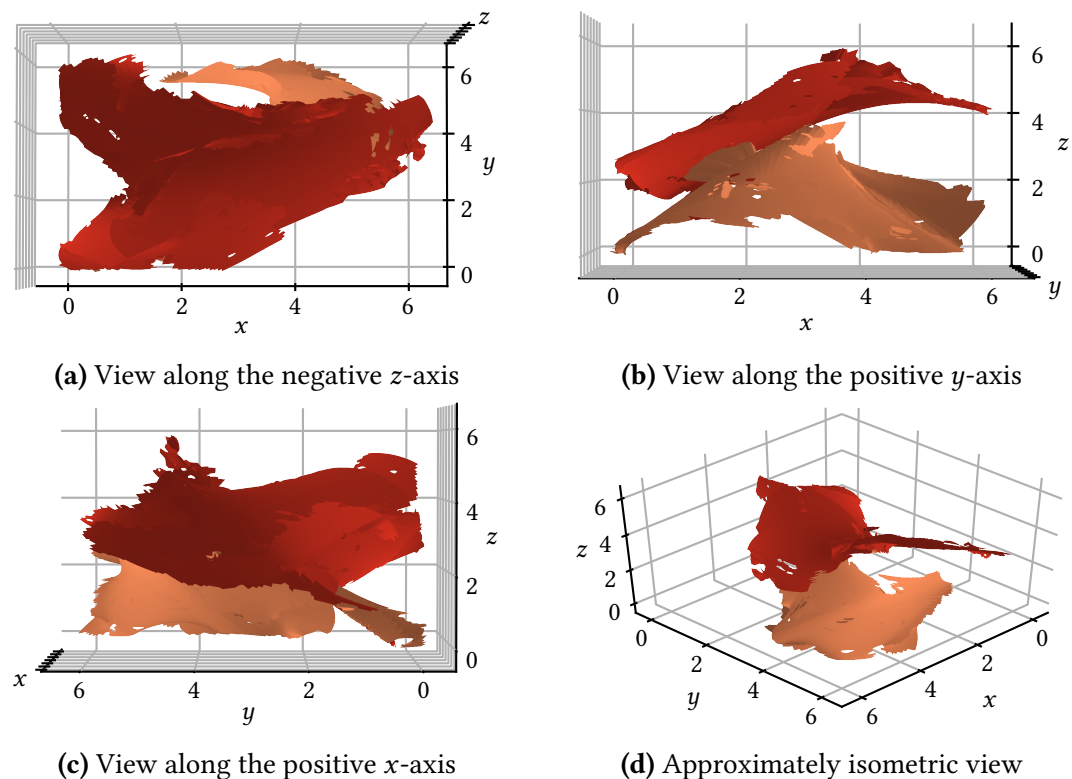
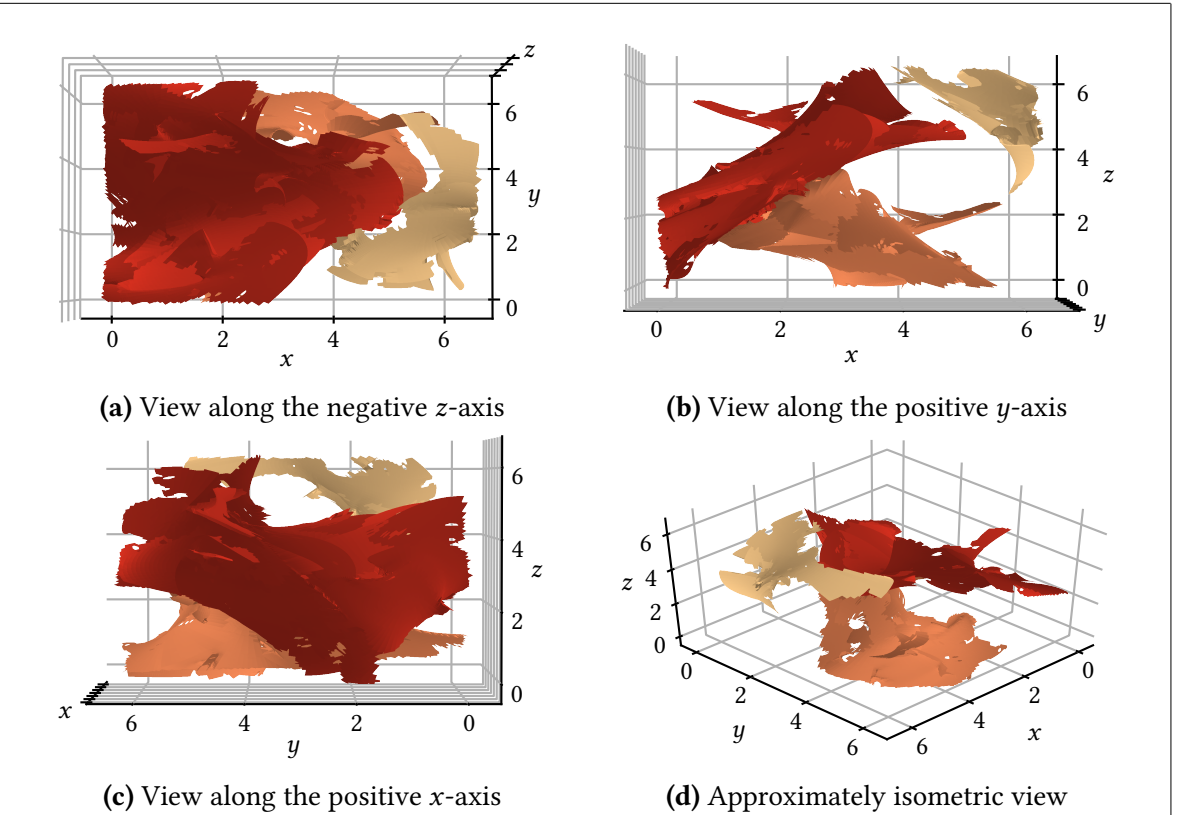
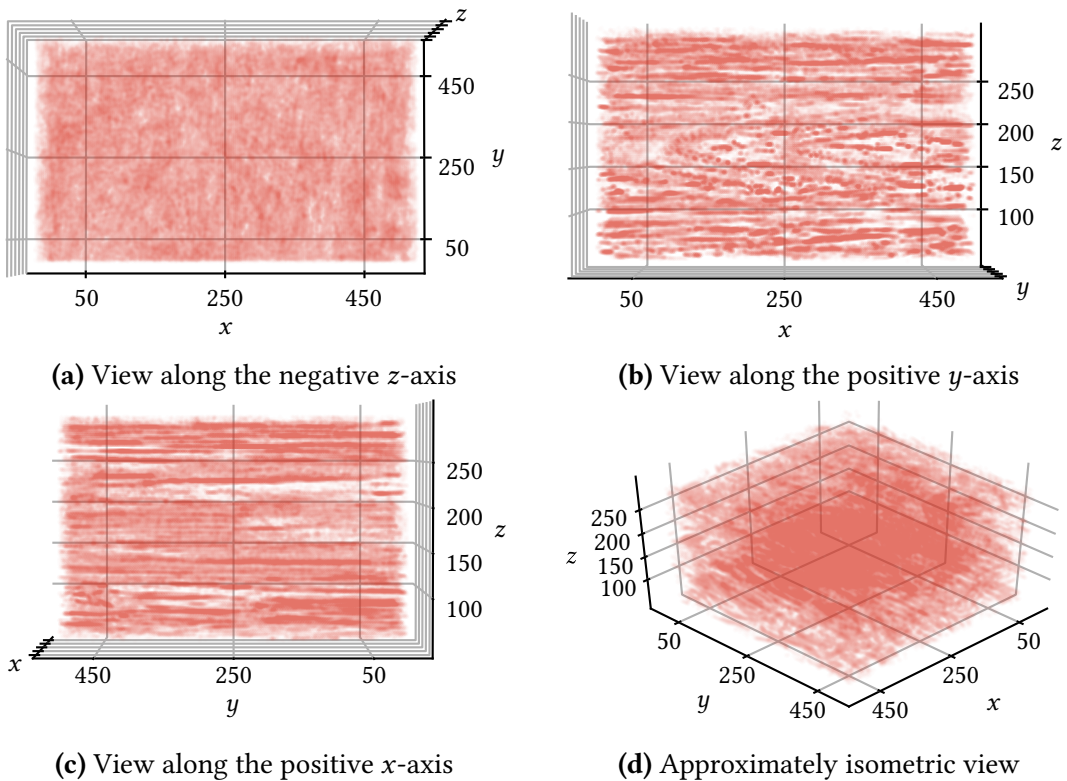


Figure 4.12: LCSs obtained for stationary ABC flow

**Figure 4.13:** LCSs obtained for dynamic ABC flow**Figure 4.14:** ABD domain obtained for gridded data. The axes have dimension meters. $z = 0$ corresponds to the sea level, increasing downwards. $\epsilon = 1$.

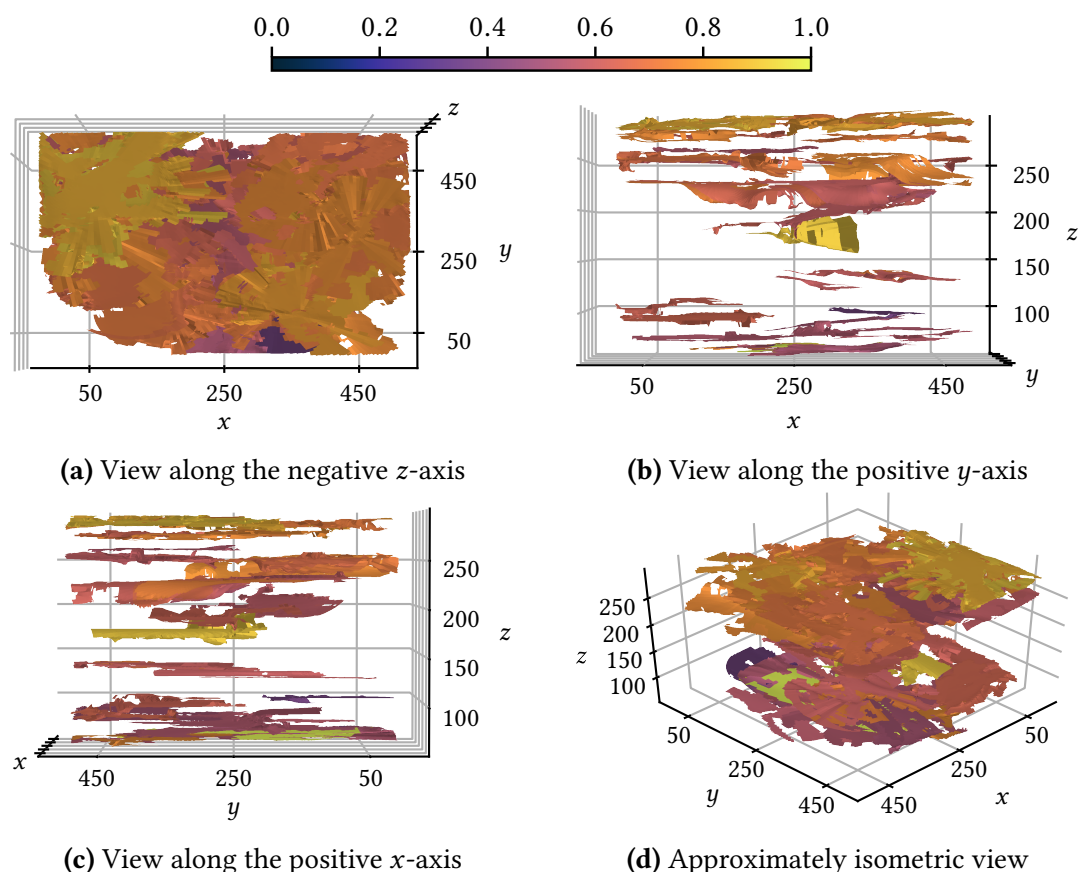


Figure 4.15: LCSs obtained for stationary ABC flow

5 Discussion

6 Conclusions

References

- Farazmand, M. and Haller, G. (2012a). "Computing Lagrangian coherent structures from their variational theory". In: *Chaos: An Interdisciplinary Journal of Nonlinear Science* 22.1, p. 013128. ISSN: 1054-1500. DOI: [10.1063/1.3690153](https://doi.org/10.1063/1.3690153).
- Farazmand, M. and Haller, G. (2012b). "Erratum and addendum to 'A variational theory of hyperbolic Lagrangian coherent structures' [Physica D 240 (2011) 547–598]". In: *Physica D: Nonlinear Phenomena* 241.4, pp. 439–441. ISSN: 0167-2789. DOI: [10.1016/j.physd.2011.09.013](https://doi.org/10.1016/j.physd.2011.09.013).
- Frisch, U. (1995). *Turbulence, the legacy of A.N. Kolmogorov*. 1st ed. Cambridge University Press. ISBN: 0-521-45103-5.
- Haller, G. (2010). "A variational theory of hyperbolic Lagrangian Coherent Structures". In: *Physica D: Nonlinear Phenomena* 240.7, pp. 547–598. ISSN: 0167-2789. DOI: [10.1016/j.physd.2010.11.010](https://doi.org/10.1016/j.physd.2010.11.010).
- Karrasch, D. (2012). "Comment on 'A variational theory of hyperbolic Lagrangian coherent structures, Physica D 240 (2011) 574–598'". In: *Physica D: Nonlinear Phenomena* 241.17, pp. 1470–1473. ISSN: 0167-2789. DOI: [10.1016/j.physd.2012.05.008](https://doi.org/10.1016/j.physd.2012.05.008).
- Oettinger, D. and Haller, G. (2016). "An autonomous dynamical system captures all LCSs in three-dimensional unsteady flows". In: *Chaos: An Interdisciplinary Journal of Nonlinear Science* 26.10. ISSN: 1054-1500. DOI: [10.1063/1.4965026](https://doi.org/10.1063/1.4965026).
- Onu, K., Huhn, F., and Haller, G. (2015). "LCS Tool: A computational platform for Lagrangian coherent structures". In: *Journal of Computational Science* 7, pp. 26–36. ISSN: 1877-7503. DOI: [10.1016/j.jocs.2014.12.002](https://doi.org/10.1016/j.jocs.2014.12.002).
- Zhao, X.-H. et al. (1993). "Chaotic and Resonant Streamlines in the ABC flow". In: *SIAM Journal on Applied Mathematics* 53.1, pp. 71–77. DOI: [10.1137/0153005](https://doi.org/10.1137/0153005).

A Appendix A